European Radiology (2019) 29:4447–4455
https://doi.org/10.1007/s00330-018-5977-y

UROGENITAL

Diffusion kurtosis imaging to assess correlations with clinicopathologic factors for bladder cancer: a comparison between the multi-*b* value method and the tensor method

Fang Wang[1,2] · Hai-Ge Chen[3] · Rui-Yun Zhang[3] · Di Jin[3] · Shuai-Shuai Xu[1] · Guang-Yu Wu[1] · Jian-Rong Xu[1]

Received: 16 August 2018 / Revised: 6 December 2018 / Accepted: 17 December 2018 / Published online: 21 January 2019

Abstract

Objectives To assess the efficacy of diffusion kurtosis imaging (DKI) in differentiating low-grade from high-grade tumors and evaluating the aggressiveness of bladder cancer.

Methods From January 2017 to July 2017, 35 patients (28 males, 7 females; mean age 63 ± 9 years) diagnosed with bladder cancer underwent diffusion-weighted imaging (DWI) with two types of DKI protocols: (1) multi-*b* value ranging from 0 to 2000 s/mm^2 to obtain mean diffusivity/kurtosis (MD_b/MK_b) and (2) the tensor method with 32 directions with 3 *b* values (0, 1000, and 2000s/mm^2) to obtain mean/axial/radial diffusivity (MD_t/Da/Dr), mean/axial/radial kurtosis (MK_t/Ka/Kr), and fractional anisotropy (FA) before radical cystectomy. Comparisons between the low- and high-grade groups, non-muscle-invasive bladder cancer (NMIBC), and muscle-invasive bladder cancer (MIBC) were performed with the areas under the receiver operating characteristic curves (AUCs).

Results The MK_t and Kr values were significantly ($p = 0.017$ and $p = 0.048$) higher in patients with high-grade bladder tumors than in those with low-grade tumors. The MK_t, Kr, and MK_b values were significantly ($p = 0.022$, $p = 0.000$, and $p = 0.044$, respectively) higher in patients with MIBC than in those with NMIBC, while no significant differences ($p > 0.05$) were found in other values. The AUC of Kr (0.883) was the largest and was significantly higher than those of other metrics (all $p < 0.05$) for differentiating MIBC from NMIBC, with a sensitivity and specificity of 81.8% and 91.7%, respectively.

Conclusions Kurtosis metrics performed better than diffusion metrics in differentiating MIBC from NMIBC, and directional kurtosis and Kr metrics may also have great potential in providing additional information regarding bladder cancer invasiveness.

Key Points

- *Kurtosis metrics performed better than diffusion metrics in differentiating muscle-invasive bladder cancer (MIBC) from non-muscle-invasive bladder cancer (NMIBC).*
- *Directional kurtosis can provide additional directional microstructural information regarding bladder cancer invasiveness.*

Keywords Cystectomy · Urinary bladder neoplasms · Magnetic resonance imaging · Diffusion magnetic resonance imaging · Diffusion tensor imaging

Fang Wang and Hai-Ge Chen contributed equally to this article.

✉ Guang-Yu Wu
gywurenji@126.com

✉ Jian-Rong Xu
JRxurenji@126.com

[1] Department of Radiology, Ren Ji Hospital, School of Medicine, Shanghai Jiao Tong University, No.1630, Dongfang road, Pudong, Shanghai 200127, China

[2] Department of Radiology, Tongji Hospital, School of Medicine, Tongji University, Shanghai 200065, China

[3] Department of Urology, Ren Ji Hospital, School of Medicine, Shanghai Jiao Tong University, Shanghai 200127, China

Abbreviations

ADC	Apparent diffusion coefficient
AUC	Area under the receiver operating characteristic curve
CLLS	Constrained linear least-square
Da	Axial diffusivity
DKT	Diffusion kurtosis tensor
Dr.	Radial diffusivity
DTI	Diffusion tensor imaging
DWI	Diffusion-weighted imaging
FA	Fractional anisotropy
ICC	Intraclass correlation coefficient
Ka	Axial kurtosis

Kr	Radial kurtosis
MIBC	Muscle-invasive bladder cancer
MK	Mean kurtosis
MRI	Magnetic resonance imaging
NMIBC	Non-muscle-invasive bladder cancer
ROC	Receiver operator characteristic
TUR	Transurethral resection

Bladder cancer, one of the most common malignant urothelial carcinomas, is the fourth most common cancer in males and the tenth in females [1]. Precise preoperative evaluation of bladder cancer could guide proper treatment and predict the prognosis. Tumor pathologic assessment may be the golden standard for bladder cancer grading and staging [2]. However, bladder tumor biopsies reflecting the focal lesions instead of the whole tumor may cause errors. Therefore, imaging studies could play a vital role in evaluating bladder cancer.

Magnetic resonance imaging (MRI), a non-invasive imaging modality, has been widely used in clinical practice for bladder cancer diagnosis. The apparent diffusion coefficient (ADC) obtained from diffusion-weighted imaging (DWI) could provide useful information for grading and staging bladder tumors [2–7]. The ADCs of high-grade bladder tumors and muscle-invasive bladder cancer (MIBC) are lower than those of low-grade tumors and non-muscle-invasive bladder cancer (NMIBC). However, there is confounding overlap of broad ADC ranges because of variations in the equipment [8]. Therefore, it is urgent to improve the performance of imaging modalities in grading and staging bladder tumors.

Diffusion kurtosis imaging (DKI) is an advanced non-Gaussian modality that can quantify the deviation from a Gaussian distribution. Compared to conventional DWI, DKI could provide additional information on non-Gaussian diffusion, which is believed to be related to irregularity and heterogeneity of cellular microstructures [9]. In this study, we investigated whether DKI parameters could differentiate low-grade from high-grade tumors and evaluate the aggressiveness of bladder cancer, and the ability to assess the grade and invasiveness of two different protocols based on the diffusion tensor method and the multi-*b* value method was also compared.

Materials and methods

The present study was a retrospective study. The protocols of this study were approved by the institutional review board, and informed consent was obtained from all patients. Forty-six patients with hematuresis or a mass detected by ultrasound who were suspected to have bladder cancer underwent MRI with a protocol including T1WI, T2WI, and DWI with (1) multi-*b* values ranging from 0 to 2000 s/mm^2 and (2) the tensor method with 32 directions with 3 *b* values (0, 500, and 1000 s/mm^2) before transurethral resection (TUR) from January 1, 2017, to July 31, 2017. Patients who underwent radical cystectomy after imaging the pathologically confirmed bladder cancer were enrolled in this study. Patients with contraindications for MRI, such as claustrophobia and the presence of an intrauterine device, a pacemaker, or metallic prostheses; images with severe motion artifacts; and pathologically confirmed carcinoma in situ (no visible lesions on DWI) or benign lesions were excluded from this study (Fig. 1, flowchart summarizing patient selection).

MRI protocols

All patients underwent pelvic MRI with the DWI protocol on a 3.0-TMR scanner (Ingenia; Philips Healthcare) with a Torso coil. Detailed information of the MRI protocol is listed in Table 1. The duration of the MRI examination is approximately 24 min. The DTI-based sequence takes approximately 6 min, and the multi-*b* value sequence takes approximately 8 min. All of the patients were instructed not to urinate for at least 1 h to achieve moderate distension of the urinary bladder.

Image analysis

All digital images were transferred to MATLAB 2014a (MathWorks) for further analysis. All ROIs were drawn by two radiologists (8 and 4 years of experience in pelvic MRI) who were blinded to the pathological outcomes. ROIs were placed by different methods based on DW images ($b = 0$ s/mm^2) and included the most restricted portions on DW images ($b = 1000$ s/mm^2) based on tensor imaging. For each case, ROIs for DKI fitting were placed over the entire largest lesion, avoiding necrotic areas (Figs. 5 and 6). All ROIs were fitted to the diffusion kurtosis tensor (DKT) imaging model described by Eq. (1) using a constrained linear least-square (CLLS) method [10]. DWI data, including those from the multi-*b* value group and tensor group, were analyzed quantitatively according to the corresponding mathematical expressions as follows:

1. DKI with tensor data:

$$\ln[S(n,b)/S_0] = -b\sum_{i=1}^{3}\sum_{j=1}^{3} n_i n_j D_{ij} + \frac{1}{6}b^2\overline{D}^2\sum_{i=1}^{3}\sum_{j=1}^{3}\sum_{k=1}^{3}\sum_{l=1}^{3} n_i n_j n_k n_l W_{ijkl} \quad (1)$$

where $S(n,b)$ is the diffusion signal intensity for diffusion weighting b and diffusion-encoding direction n, S_0 is the signal intensity for b_0, and D_{ij} and W_{ijkl} are components of the

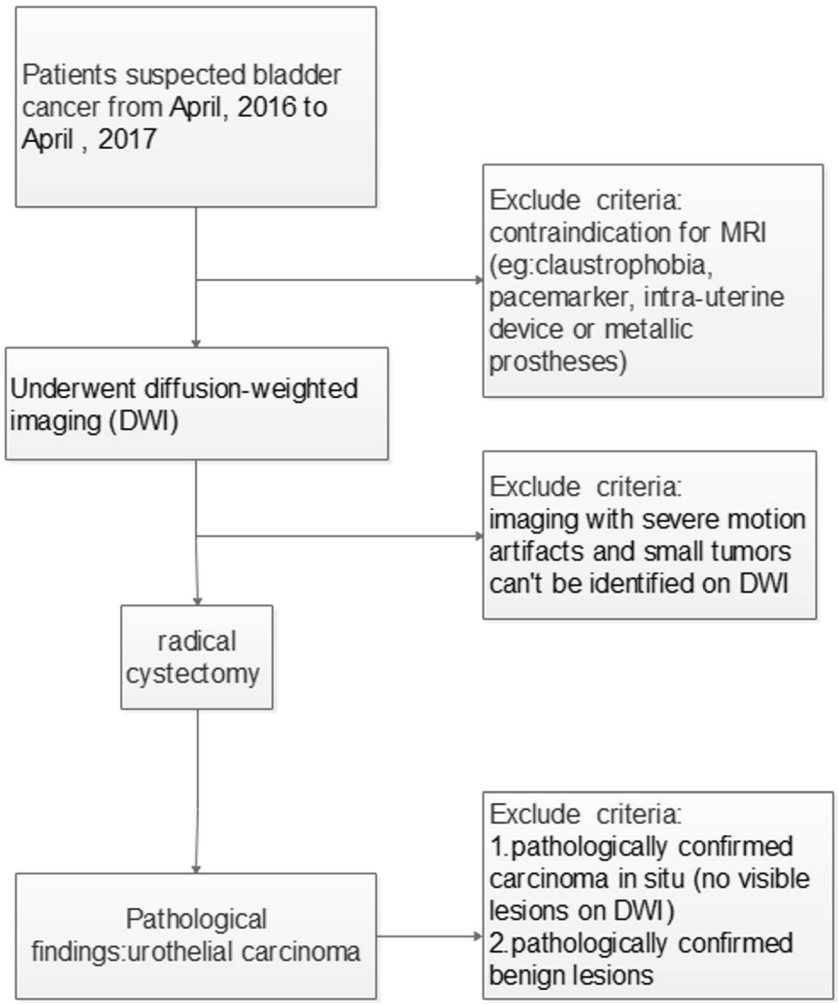

Fig. 1 Flowchart summarizing patient selection

diffusion and kurtosis tensor, respectively. With our DKT protocol, we obtained parametric maps related to diffusional kurtosis: MK_t (apparent kurtosis coefficient averaged over all directions), Kr (kurtosis along the radial direction), and Ka (kurtosis along the axial direction). Conventional DTI-based metrics were also derived, including MD_t and fractional anisotropy (FA), with the former measuring the magnitude of diffusion and the latter quantifying the preferential directionality of water diffusion. Radial diffusivity (Dr) and axial diffusivity (Da) maps were also derived to characterize the directional properties of diffusivity. Details on the computation of these metrics have been described previously [11].

2. DKI with multi-*b* value data

$$S(b) = S_0 \exp\left(-bMD_b + \frac{1}{6}b^2 MD_b{}^2 MK_b\right) \quad (2)$$

where MD_b is the mean diffusivity and MK_b is the dimensionless metric mean kurtosis expressing the deviation from Gaussian distribution.

Pathology

Histological results were independently evaluated by two pathologists according to the WHO 2004 classification, and consensus was reached by consulting another pathologist when disagreement occurred.

Statistical evaluation

Statistical analyses were carried out using SPSS 20.0 (SPSS Inc.). The mean ± standard deviation is used to express continuous variables. Interobserver agreement of all these metrics was evaluated by the intraclass correlation coefficient (ICC). Independent samples *t* tests were used to compare differences between the low- and high-grade groups and between the NMIBC and MIBC groups. Receiver operating characteristic (ROC) curves were drawn to compare the areas of these parameters. The $p < 0.05$ was considered statistically significant.

Table 1 Magnetic resonance imaging (MRI) protocol for tumor assessment

MRI protocol	MRI sequences		
	T1-weighted	T2-weighted	DWI
Plane	Axial	Axial, sagittal	Axial
Fat suppressed	No	Yes	No
Time to repeat (ms)	534	4000	6000
Time to echo	8	110	70
Thickness (mm)	3	3	3
FOV (cm)	30 × 30	22 × 22	20 × 30
Matrix (mm × mm)	300 × 226	276 × 239	80 × 142
Intersection gap (mm)	1	1	0.3
Number of excitation	2	2	2
Other			Multi-*b* value (9 *b* values 0, 50, 100, 150, 200, 500, 800, 1000, 2000 s/mm^2)
			Tensor method with 32 direction (3 *b* values 0, 500, and 1000s/mm^2)

FOV field of view, *DWI* diffusion-weighted imaging

Results

Histopathological findings

A total of 35 patients (28 males, 7 females; mean age 63 ± 9 years) were enrolled in this study. There were 11 low-grade and 24 high-grade bladder tumors and 24 cases of non-muscle-invasive bladder cancer (NMIBC) and 11 cases of muscle-invasive bladder cancer (MIBC) based on these pathological findings.

Interobserver agreement

The measurement consistency between two observers was evaluated by the ICC, which demonstrated excellent agreement between two observers for the parameters derived from multi-*b* values and the tensor method (ICC 0.928–0.998).

Correlations between MR parameters from two protocols

Directional diffusion metrics (MD_t, Da, Dr) were significantly ($p < 0.01$) correlated with the MD_b, and the directional kurtosis metrics (MK_t, Ka, Kr) were significantly ($p < 0.01$) correlated with the MK_b (Table 2).

Comparisons of MR parameters between the low-grade and high-grade bladder tumors

The MK_t and Kr values were significantly ($p < 0.05$) higher in patients with high-grade bladder tumors (0.693 ± 0.135 and 0.7 ± 0.129) than in those with low-grade bladder tumors (0.581 ± 0.091 and 0.606 ± 0.118) (Table 3; Fig. 2). There were no significant ($p > 0.05$) differences in other values between high- and low-grade bladder tumors.

Comparisons of MR parameters between the MIBC and NMIBC groups

The MK_t, Kr, and MK_b values were significantly ($p < 0.05$) higher in patients of the MIBC group (0.732 ± 0.115, 0.794 ± 0.111, and 0.749 ± 0.238, respectively) than in those of the NMIBC group (0.624 ± 0.127, 0.626 ± 0.155, and 0.597 ± 0.19, respectively) (Table 3; Fig. 3). There were no significant ($p > 0.05$) differences in other values between the MIBC and NMIBC groups.

Diagnostic performance for DKI parameters between the NMIBC and MIBC groups

The areas under the receiver operating characteristic curves of Kr values (0.883) were significantly ($p < 0.05$) larger than all of the other values for differentiating MIBC from NMIBC, and the sensitivity and specificity were 81.8 and 91.7, respectively (Table 4; Figs. 4, 5, and 6).

Discussion

In this study, we found that kurtosis metrics in the MIBC group were significantly higher than those in the NMIBC group, and the performance of kurtosis metrics was superior to that of diffusion metrics for differentiating MIBC from NMIBC. MIBC is heterogeneous with atypical cells and is characterized by endothelial proliferation, vascular hyperplasia, necrosis, and hemorrhage [12], while NMIBC consists of more homogeneous clusters of well-differentiated cells with fewer diffusion barriers. Higher kurtosis metrics indicate more heterogeneous and complex microstructures [13, 14], which could be the reasonable explanation for our results. Although directional kurtosis metrics (MK_t, K_a, Kr) have good correlations with mean kurtosis metrics (MK_b), we found that kurtosis in the radial direction performed better than other metrics in differentiating MIBC from NMIBC. In our study, Kr was defined as kurtosis in the radial direction, which is perpendicular to the axial direction (vector with largest diffusivity); we posit that improved performance in tumor characteristics with Kr may mainly be due to the evaluation of diffusion kurtosis in

Table 2 Correlations between MR parameters from two protocols

		MK_t	MK_b	Ka	Kr	MD_t	MD_b	Da	Dr	FA
MK_t	*r*	1	0.443	0.68	0.736	− 0.795	− 0.438	− 0.786	− 0.782	− 0.289
	p		0.008	0.000	0.000	0.000	0.010	0.000	0.000	0.092
MK_b	*r*	0.443	1	0.467	0.576	− 0.505	− 0.583	− 0.561	− 0.450	− 0.428
	p	0.008		0.005	0.000	0.002	0.000	0.000	0.007	0.01
Ka	*r*	0.68	0.467	1	0.424	− 0.718	− 0.335	− 0.780	− 0.655	− 0.652
	p	0.000	0.005		0.011	0.000	0.053	0.000	0.000	0.000
Kr	*r*	0.736	0.576	0.424	1	− 0.59	− 0.45	− 0.601	− 0.567	− 0.3
	p	0.000	0.000	0.011		0.000	0.008	0.000	0.000	0.08
MD_t	*r*	− 0.795	− 0.505	− 0.718	− 0.59	1	0.515	0.980	0.989	0.227
	p	0.000	0.002	0.000	0.000		0.002	0.000	0.000	0.189
MD_b	*r*	− 0.438	− 0.583	− 0.335	− 0.45	0.515	1	0.538	0.484	0.242
	p	0.01	0.000	0.053	0.008	0.002		0.001	0.004	0.169
Da	*r*	− 0.786	− 0.561	− 0.78	− 0.601	0.98	0.538	1	0.941	0.404
	p	0.000	0.000	0.000	0.000	0.000	0.001		0.000	0.016
Dr	*r*	− 0.782	− 0.45	− 0.655	− 0.567	0.989	0.484	0.941	1	0.091
	p	0.000	0.007	0.000	0.000	0.000	0.004	0.000		0.604
FA	*r*	− 0.289	− 0.428	− 0.652	− 0.3	0.227	0.242	0.404	0.091	1
	p	0.092	0.01	0.000	0.08	0.189	0.169	0.016	0.604	

MK_b mean kurtosis (obtained from multi-*b* value method), *MK_t* mean kurtosis (obtained from tensor method), *Ka* axial kurtosis, *Kr* radial kurtosis, *MD_b* mean diffusivity (obtained from multi-*b* value method), *MD_t* mean diffusion (obtained from tensor method), *Da* axial diffusivity, *Dr* radial diffusivity, *FA* fractional anisotropy

that specific direction, which excluded information on the vector with the largest diffusivity.

However, there were no significant differences in diffusion metrics in the low- and high-grade groups, and the performance of kurtosis metrics was not significantly superior to diffusion metrics for differentiating high-grade from low-grade tumors. These may be attributed to several histomorphologic criteria, including variations in nuclear size, shape, and polarity as well as chromatin distribution patterns and the presence or absence of nucleoli and mitotic figures, which were somehow subjective. And using a complex combination of these factors to grade bladder tumors may result in substantial interobserver variability [15]. Besides, there were no significant differences in FA between low- and high-grade bladder tumors or between NMIBC and MIBC. As the restriction of diffusion may deviate in all directions in the solid region of the tumor to a similar degree, tumors of different grades differ in the sphere size of the diffusion range instead of its shape. Therefore, FA is of little value in assessing both the grade and invasiveness of bladder cancer.

Table 3 Comparisons between different histological groups

Parameter	LG	HG	*p* value	NMIBC	MIBC	*p* value
MD_t	2.200 ± 0.321	1.994 ± 0.330	0.093	2.121 ± 0.317	1.923 ± 0.352	0.109
Da	2.648 ± 0.423	2.364 ± 0.421	0.08	2.535 ± 0.424	2.274 ± 0.426	0.101
Dr	1.976 ± 0.28	1.809 ± 0.291	0.12	1.913 ± 0.272	1.748 ± 0.322	0.12
MK_t	0.581 ± 0.091	0.693 ± 0.135	0.017	0.624 ± 0.127	0.732 ± 0.115	0.022
Ka	0.465 ± 0.149	0.561 ± 0.230	0.06	0.536 ± 0.191	0.624 ± 0.206	0.225
Kr	0.606 ± 0.118	0.700 ± 0.129	0.048	0.626 ± 0.155	0.794 ± 0.111	0.000
FA	0.205 ± 0.04	0.190 ± 0.041	0.335	0.198 ± 0.041	0.188 ± 0.043	0.515
MD_b	1.195 ± 0.380	0.999 ± 0.196	0.054	1.097 ± 0.293	0.972 ± 0.214	0.216
MK_b	0.567 ± 0.193	0.680 ± 0.220	0.133	0.597 ± 0.190	0.749 ± 0.238	0.044

LG low-grade, *HG* high-grade, *NMIBC* non-muscle-invasive bladder cancer, *MIBC* muscle-invasive bladder cancer, *MK_b* mean kurtosis (obtained from multi-*b* value method), *MK_t* mean kurtosis (obtained from tensor method), *Ka* axial kurtosis, *Kr* radial kurtosis, *MD_b* mean diffusivity (obtained from multi-*b* value method), *MD_t* mean diffusivity (obtained from tensor method), *Da* axial diffusivity, *Dr* radial diffusivity, *FA* fractional anisotropy

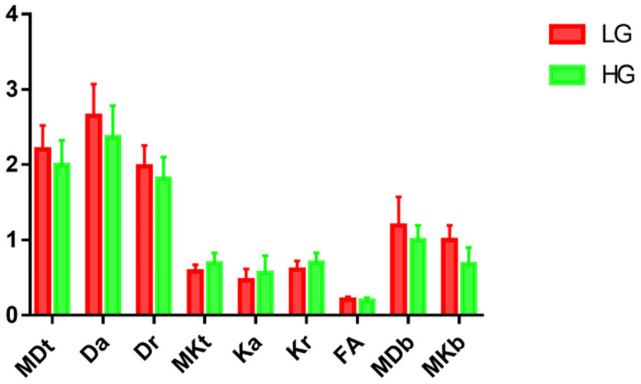

Fig. 2 Comparisons of MR parameters between the low-grade and high-grade bladder tumors. MD_t, MD_b, Da, and Dr are presented in 10^{-3} mm^2/s, and the remaining parameters are dimensionless

Multi-*b* values [16–20] and the tensor method [13, 21–24] are two common types of DKI protocols that have been performed in previous studies in many organs, including the brain, breast, prostate, and kidney [13, 16–24]. A previous study [20] investigated the value of DKI in grading bladder cancer and found that the diffusion in bladder cancer followed a non-Gaussian distribution and that bladder cancer may be graded based on kurtosis. The previous study used a non-tensor-based method with a proposed non-linear least squares fitting procedure using a multi-*b* value–based method instead of a tensor-based method, which raises several issues regarding the accuracy and precision of the estimated metrics. DKT imaging is an extension of diffusion tensor imaging (DTI) that quantifies non-Gaussian water diffusion by acquiring data for at least two non-zero diffusion gradient factors (*b* values) in at least 15 independent directions [11]. The kurtosis metrics (i.e., the mean kurtosis (MK), axial kurtosis (Ka), and radial kurtosis (Kr)) and the conventional diffusion metrics (i.e., the mean diffusivity (MD), axial diffusivity (Da), radial diffusivity (Dr), and fractional anisotropy (FA)) can be derived from DKT imaging data simultaneously [11]. The Ka and Kr are parallel and perpendicular to the main direction of diffusion, respectively, while the MK is the average kurtosis over all diffusion

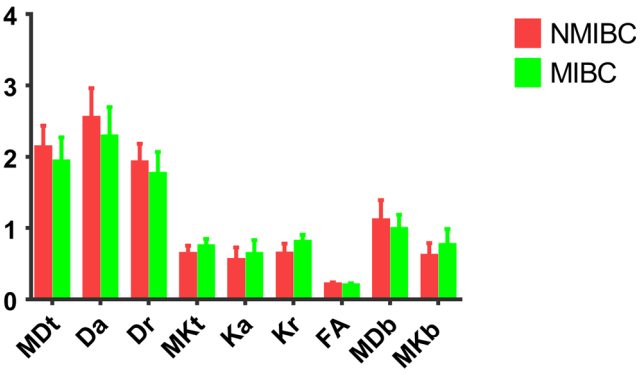

Fig. 3 Comparisons of MR parameters between the MIBC and NMIBC groups. MD_t, MD_b, Da, and Dr are presented in 10^{-3} mm^2/s, and the remaining parameters are dimensionless

Table 4 Diagnostic performance for DKI parameters between the NMIBC and MIBC groups

Parameters	Cutoff	AUC	Sensitivity, 100%	Specificity, 100%
MK_t	0.700	0.754	72.7	83.3
Ka	0.563	0.621	54.5	70.8
Kr	0.700	0.883	81.8	91.7
MD_t	2.112	0.678	78.9	54.2
Da	2.571	0.663	90.9	40.8
Dr	1.873	0.648	70	54.2
FA	0.211	0.557	66.3	37.5
MK_b	0.702	0.693	54.5	77.8
MD_b	1.1	0.601	90.9	38.5

MK_b mean kurtosis (obtained from multi-*b* value method), *MK_t* mean kurtosis (obtained from tensor method), *Ka* axial kurtosis, *Kr* radial kurtosis, *MD_b* mean diffusivity (obtained from multi-*b* value method), *MD_t* mean diffusivity (obtained from tensor method), *Da* axial diffusivity, *Dr* radial diffusivity, *FA* fractional anisotropy

directions [11]. Because diffusion kurtosis is a tensorial quantity, it can provide additional information on diffusion kurtosis in a particular direction in addition to the MK value, while the non-tensor-based method precludes the possibility of evaluating Kr and Kx. The application of DKI with multidirectional diffusion tensor in bladder tumors has not been fully elucidated. Thus, in this study, we compared the ability of these two types of DKI protocols to grade and evaluate the invasiveness of bladder cancer. Besides, the anisotropic directionality of diffusion and kurtosis behavior with tensor was also investigated in our study. A study showed that although MK is sensitive in the detection of Huntington's disease, it can lose sensitivity and specificity in probing the directional changes of pathological tissue [25]. In addition, the results from a study indicated that directional kurtosis, including Kr and Ka, can provide additional directional microstructural information in

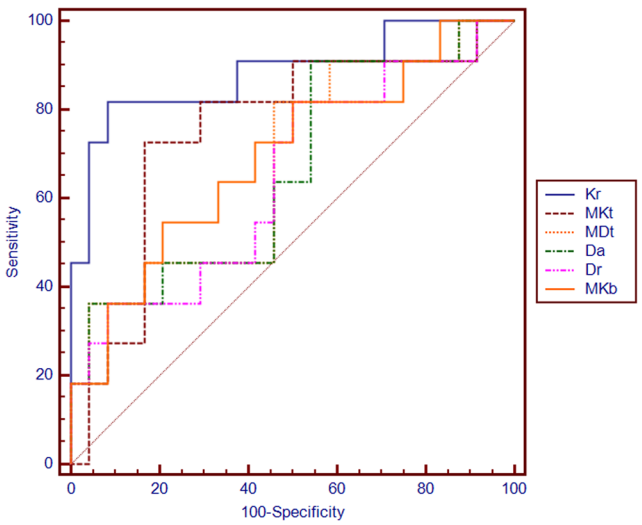

Fig. 4 ROC curves of MR parameters for discriminating MIBC from NMIBC

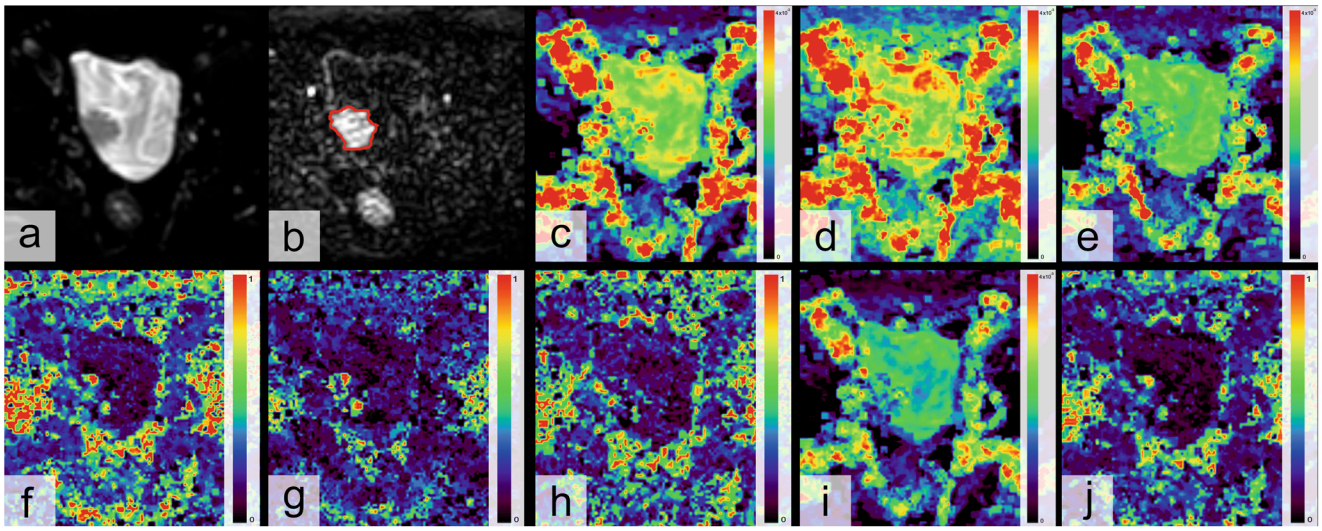

Fig. 5 Images acquired from a 61-year-old male diagnosed with low-grade and non-muscle-invasive bladder cancer confirmed by pathological findings. **a** Diffusion-weighted imaging with a *b* value of 0 s/mm^2 shows a papillary margin on the right lateral bladder wall. **b** Diffusion-weighted imaging with a *b* value of 1000 s/mm^2 based on tensor imaging. Directional (**c**–**e**) MD mapping (MD_t, Da, Dr) and (**f**–**h**) MK mapping (MK_t, Ka, Kr) derived from the tensor method. **i** MD mapping (MD_b) and (**j**) MK mapping (MK_b) derived from the multi-*b* method

characterizing neural tissues [26]. Our study indicated that direction-specific kurtosis could also exhibit specific information in tumor diagnosis compared with MK, which addresses the mean kurtosis and would overly concern the generality of the tumor [27]. Thus, the application of the tensor method in some respects is preferable despite requiring more time than the multi-*b* value method. To the best of our knowledge, this report was the first to demonstrate the significance of the direction-specific kurtosis metric in assessing the invasiveness of tumors. Although the result seems to be quite promising for differentiating MIBC from NMIBC, the exact pathological and pathophysiological indication of the direction-specific kurtosis metric still needs to be further explored.

Last but not least, appropriate *b* values should be chosen to obtain diffusion kurtosis with a reliable curve fitting. In the multi-*b* value method, we used the protocol with *b* values ranging from 0~2000 s/mm^2 based on the previous study [20]. However, for the tensor method, if we chose 2000s/mm^2 as the largest *b* value, the scanning time may increase sharply, potentially resulting in a time-consuming method that may be difficult to endure by patients withholding urine; in addition, this method may not be favored based on the need

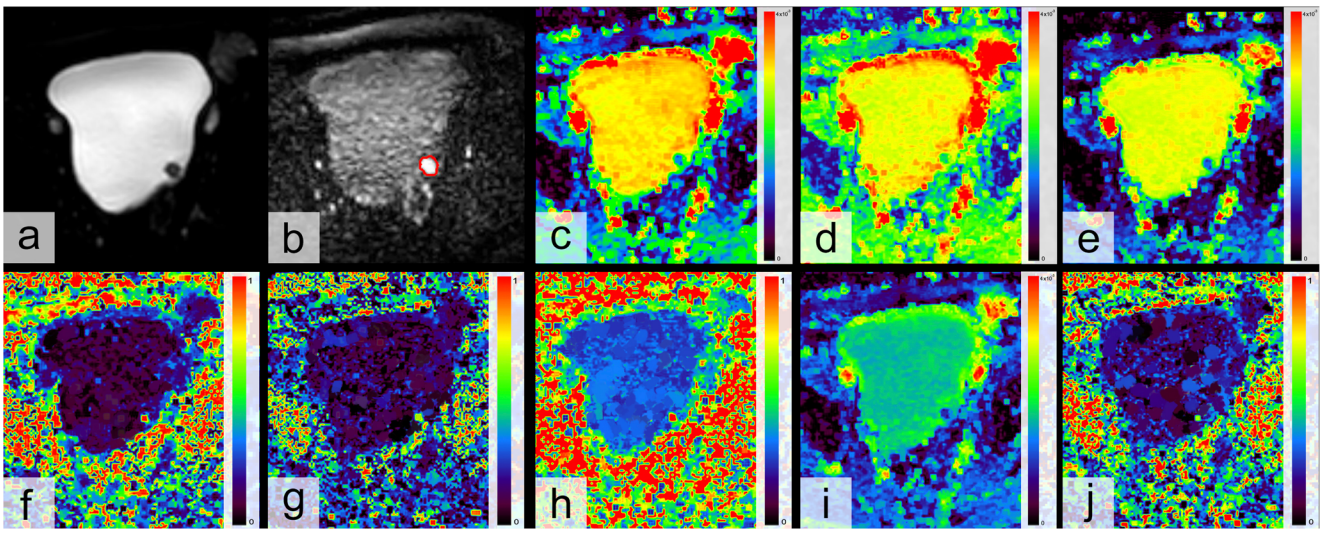

Fig. 6 Images acquired from a 72-year-old male diagnosed with high-grade and muscle-invasive bladder cancer confirmed by pathological findings. **a** Diffusion-weighted imaging with a *b* value of 0 s/mm^2 shows a nodular margin on the left lateral bladder wall. **b** Diffusion-weighted imaging with a *b* value of 1000 s/mm^2 based on tensor imaging. Directional (**c**–**e**) MD mapping (MD_t, Da, Dr) and (**f**–**h**) MK mapping (MK_t, Ka, Kr) derived from the tensor method. **i** MD mapping (MD_b) and (**j**) MK mapping (MK_b) derived from the multi-*b* method

for efficiency in clinical work. Meanwhile, a previous study demonstrated that diffusional kurtosis is determined by the small *b* value behavior of S(b) [11]. DKT imaging with higher *b* values reflects a different population of restricted spins that is diffusing within smaller pores. Because the *K* value represents a deviation from a Gaussian model of water motion, using DTI data collected with high *b* values (within the appropriate range of maximum *b* values for DKT imaging) is more likely to increase the robustness of the *K* estimates [11, 27]. After weighing the advantages and disadvantages, we chose 1000 s/mm^2 as the largest *b* value in our study. However, the impact of the high *b* value on DKI of bladder cancer is unknown, and further study is needed to explore the matter.

There were also several limitations in this study. First, our study was a preliminary and retrospective study with a relatively limited number of cases. Although we demonstrated the significance of direction-specific kurtosis in characterizing bladder cancer, further study is needed to better understand the underlying pathological and pathophysiological mechanisms of DKI and further validate its clinical use in the future. Second, an entire tumor-based histogram analysis may be more objective and may better reflect the heterogeneity of the whole volume than analysis at the largest single plane. However, this method may be somewhat time consuming. A previous study [28] found that the application of single-slice analysis is preferred to entire-tumor analysis in clinical practice due to its excellent repeatability and short duration. Moreover, it is reasonable to perform the analysis with the largest single plane, as it displayed excellent interobserver agreement in our study.

In conclusion, Kurtosis metrics could provide better performance than diffusion metrics in differentiating MIBC from NMIBC. In addition, directional kurtosis, Kr metrics, could potentially reveal additional directional changes in invasive bladder cancer and may be a promising biomarker of bladder cancer aggressiveness.

Funding This study has received funding from the National Natural Science Foundation of China (Youth Program Nos. 81601487, 81672514).

Compliance with ethical standards

Guarantor The scientific guarantor of this publication is Jian-Rong Xu.

Conflict of interest The authors of this manuscript declare no relationships with any companies whose products or services may be related to the subject matter of the article.

Statistics and biometry No complex statistical methods were necessary for this paper.

Informed consent Written informed consent was obtained from all subjects (patients) in this study.

Ethical approval Institutional Review Board approval was obtained.

Study subjects or cohorts overlap Study subjects or cohorts overlap have not been published previously and not under consideration for publication elsewhere, in whole or in part.

Methodology
- retrospective
- diagnostic study
- performed at one institution

References

1. Jemal A, Siegel R, Xu J, Ward E (2010) Cancer statistics, 2010. CA Cancer J Clin 60:277–300
2. Rabie E, Faeghi F, Izadpanahi MH, Dayani MA (2016) Role of dynamic contrast-enhanced magnetic resonance imaging in staging of bladder cancer. J Clin Diagn Res 10:TC01–TC05
3. Takeuchi M, Sasaki S, Ito M et al (2009) Urinary bladder cancer: diffusion-weighted MR imaging–accuracy for diagnosing T stage and estimating histologic grade. Radiology 251:112–121
4. Rosenkrantz AB, Mussi TC, Spieler B, Melamed J, Taneja SS, Huang WC (2012) High-grade bladder cancer: association of the apparent diffusion coefficient with metastatic disease: preliminary results. J Magn Reson Imaging 35:1478–1483
5. Dağgülli M, Onur MR, Fırdolaş F, Onur R, Kocakoç E, Orhan İ (2011) Role of diffusion MRI and apparent diffusion coefficient measurement in the diagnosis, staging and pathological classification of bladder tumors. Urol Int 87:346–352
6. Takeuchi M, Sasaki S, Naiki T et al (2013) MR imaging of urinary bladder cancer for T-staging: a review and a pictorial essay of diffusion-weighted imaging. J Magn Reson Imaging 38:1299–1309
7. Kobayashi S, Koga F, Kajino K et al (2014) Apparent diffusion coefficient value reflects invasive and proliferative potential of bladder cancer. J Magn Reson Imaging 39:172–178
8. El-Assmy A, Abou-El-Ghar ME, Refaie HF, Mosbah A, El-Diasty T (2012) Diffusion-weighted magnetic resonance imaging in follow-up of superficial urinary bladder carcinoma after transurethral resection: initial experience. BJU Int 110:E622–E627
9. Jensen JH, Helpern JA, Ramani A, Lu H, Kaczynski K (2005) Diffusional kurtosis imaging: the quantification of non-Gaussian water diffusion by means of magnetic resonance imaging. Magn Reson Med 53:1432–1440
10. Tabesh A, Jensen JH, Ardekani BA, Helpern JA (2011) Estimation of tensors and tensor-derived measures in diffusional kurtosis imaging. Magn Reson Med 65:823–836
11. Jensen JH, Helpern JA (2010) MRI quantification of non-Gaussian water diffusion by kurtosis analysis. NMR Biomed 23:698–710
12. O'Brien T, Cranston D, Fuggle S, Bicknell R, Harris AL (1995) Different angiogenic pathways characterize superficial and invasive bladder cancer. Cancer Res 55:510–513
13. Van Cauter S, Veraart J, Sijbers J et al (2012) Gliomas: diffusion kurtosis MR imaging in grading. Radiology 263:492–501
14. Tietze A, Hansen MB, Østergaard L et al (2015) Mean diffusional kurtosis in patients with glioma: initial results with a fast imaging method in a clinical setting. AJNR Am J Neuroradiol 36:1472–1478
15. May M, Brookman-Amissah S, Roigas J et al (2010) Prognostic accuracy of individual uropathologists in noninvasive urinary bladder carcinoma: a multicentre study comparing the 1973 and 2004 World Health Organisation classifications. Eur Urol 57:850–858

16. Nogueira L, Brandão S, Matos E et al (2014) Application of the diffusion kurtosis model for the study of breast lesions. Eur Radiol 24:1197–1203
17. Suo S, Chen X, Wu L et al (2014) Non-Gaussian water diffusion kurtosis imaging of prostate cancer. Magn Reson Imaging 32:421–427
18. Rosenkrantz AB, Sigmund EE, Johnson G et al (2012) Prostate cancer: feasibility and preliminary experience of a diffusional kurtosis model for detection and assessment of aggressiveness of peripheral zone cancer. Radiology 264:126–135
19. Roethke MC, Kuder TA, Kuru TH et al (2015) Evaluation of diffusion kurtosis imaging versus standard diffusion imaging for detection and grading of peripheral zone prostate cancer. Invest Radiol 50:483–489
20. Suo S, Chen X, Ji X et al (2015) Investigation of the non-Gaussian water diffusion properties in bladder cancer using diffusion kurtosis imaging: a preliminary study. J Comput Assist Tomogr 39:281–285
21. Jensen JH, Falangola MF, Hu C et al (2011) Preliminary observations of increased diffusional kurtosis in human brain following recent cerebral infarction. NMR Biomed 24:452–457
22. Pentang G, Lanzman RS, Heusch P et al (2014) Diffusion kurtosis imaging of the human kidney: a feasibility study. Magn Reson Imaging 32:413–420
23. Veraart J, Poot DH, Van Hecke W et al (2011) More accurate estimation of diffusion tensor parameters using diffusion kurtosis imaging. Magn Reson Med 65:138–145
24. Quentin M, Pentang G, Schimmöller L et al (2014) Feasibility of diffusional kurtosis tensor imaging in prostate MRI for the assessment of prostate cancer: preliminary results. Magn Reson Imaging 32:880–885
25. Van Camp N, Blockx I, Verhoye M et al (2009) Diffusion tensor imaging in a rat model of Parkinson's disease after lesioning of the nigrostriatal tract. NMR Biomed 22:697–706
26. Hui ES, Cheung MM, Qi L, Wu EX (2008) Towards better MR characterization of neural tissues using directional diffusion kurtosis analysis. Neuroimage 42:122–134
27. Wu G, Zhao Z, Yao Q et al (2018) The study of clear cell renal cell carcinoma with MR diffusion kurtosis tensor imaging and its histopathologic correlation. Acad Radiol 25:430–438
28. Priola AM, Priola SM, Gned D et al (2017) Diffusion-weighted quantitative MRI of pleural abnormalities: intra- and interobserver variability in the apparent diffusion coefficient measurements. J Magn Reson Imaging 46:769–782